

Topological semimetals and topological insulators in rare earth monopnictides

Minggang Zeng^{†1,2}, Chen Fang^{†3}, Guoqing Chang^{1,2}, Yu-An Chen³,

Timothy Hsieh³, Arun Bansil⁴, Hsin Lin^{*1,2} and Liang Fu^{**3}

¹Centre for Advanced 2D Materials and Graphene Research Centre,
National University of Singapore, Singapore 117546

²Department of Physics, National University of Singapore, Singapore 117542

³Department of Physics, Massachusetts Institute of Technology, Cambridge, Massachusetts 02139, USA and

⁴Department of Physics, Northeastern University, Boston, Massachusetts 02115, USA

We use first principles calculations to study the electronic properties of rock salt rare earth monopnictides $\text{La}X$ ($X = \text{N}, \text{P}, \text{As}, \text{Sb}, \text{Bi}$). A new type of topological band crossing termed ‘linked nodal rings’ is found in LaN when the small spin-orbital coupling (SOC) on nitrogen orbitals is neglected. Turning on SOC gaps the nodal rings at all but two points, which remain gapless due to C_4 -symmetry and leads to a 3D Dirac semimetal. Interestingly, unlike LaN , compounds with other elements in the pnictogen group are found to be topological insulators (TIs), as a result of band reordering due to the increased lattice constant as well as the enhanced SOC on the pnictogen atom. These TI compounds exhibit multi-valley surface Dirac cones at three \bar{M} -points on the (111)-surface.

The discovery of three-dimensional (3D) Dirac semimetals and Weyl semimetals, both theoretically[1–9] and experimentally[10–17], attracts great interest and effort into the emergent field of topological semimetals (TSM). A d -dimensional topological semimetal has Fermi surfaces of reduced dimensions below $d - 1$. In 3D, the Fermi surface of a topological semimetal is constituted of points or lines instead of surfaces. The new types of Fermi surfaces is a result of robust band crossings, or topological band crossings, between the conduction and the valence bands, protected by topology and/or symmetry. Topological semimetals have distinct physical properties such as surface Fermi arcs, negative magnetoresistance and topologically nontrivial spin texture near the Fermi surface.

With the only exception of 3D Weyl semimetals, the stability of all TSM phases requires the presence of symmetries in addition to lattice translation, such as point group or time-reversal[1–3, 18]. Breaking these symmetries in different ways typically drives the system into distinct topological phases: breaking TRS in a 2D Dirac semimetal, e.g., graphene, leads to a quantum anomalous Hall state; breaking spin rotation in the same system leads to a 2D TI; breaking time-reversal or 3D inversion a 3D Dirac semimetal splits a Dirac point into a pair of Weyl nodes resulting in a Weyl semimetal[19–24]; breaking rotation symmetry in a 3D Dirac semimetal results in a 3D TI. Therefore, a TSM could be viewed as the parent state of many interesting phases[10].

In this work, based on first-principles calculations, we predict topological semimetal and topological insulator phases in a family of lanthanum monopnictides with a simple rock salt structure: $\text{La}X$, where $X = \text{N}, \text{P}, \text{As}, \text{Sb}$ and Bi . When the small SOC is neglected in LaN , the system is an exotic TSM: the band crossing points form three intersecting nodal rings, which look like the equator and two perpendicular longitudes of a football centered at each X point, shown in Fig.1(b) (see also

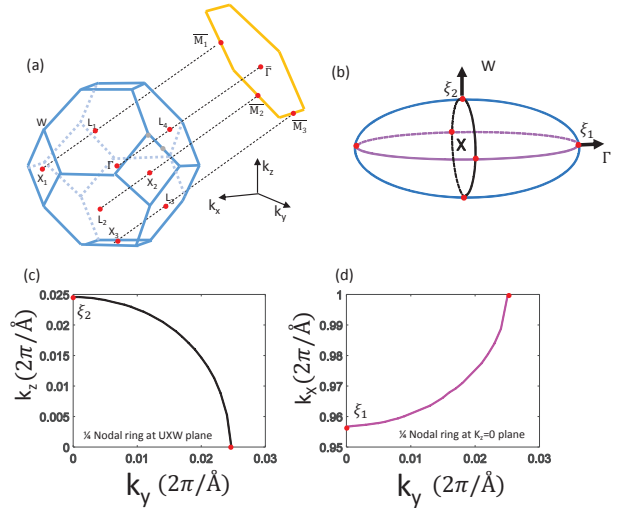


FIG. 1: (a) The 3D Brillouin zone of the face-centered cubic lattice and its projection to the surface Brillouin zone of the (111)-surface. (b) A schematic of the three nodal rings around one X-point in LaN . (c,d) The calculated configuration of the nodal rings on the yz -plane and the xy -plane, respectively. Due to symmetry, only one quarter of each ring is shown.

Ref.25 for a similar configuration of nodal lines proposed in 3D graphene networks). These nodal rings are protected by three mirror planes as well as spin rotation symmetry, and as the latter is broken by a perturbative SOC, they are gapped almost everywhere, leaving two Dirac points behind. Hence in LaN , born from the nodal ring semimetal is a Dirac semimetal with six Dirac points, two near each X-point, in the Brillouin zone (BZ). 3D Dirac semimetals have been experimentally identified in Na_3Bi and Cd_3As_2 [11–14]. Considering that the former is chemically unstable under ambient conditions, and the latter has a very complicated crystal structure, we note that LaN , being a simple binary compound with rock salt structure, has certain advantages from materi-

als perspective. In the other compounds ($X=P$, As, Sb and Bi), the bulk is a 3D TI with full direct gap. A band inversion between lanthanum d -orbitals and pnictogen p -orbitals at X -point appears in all five compounds, and hence is *not* the reason for the topological phase transition from TSM to TI. Our study shows that a significant increase in the lattice constant changes the orbital nature of the valence band from p_x -orbital to a linear combination of $p_{y,z}$ -orbitals; this change in orbital nature causes the topological distinction between a TSM in LaN and a TI in the other monopnictides. To demonstrate the TI phase, we calculate the band structure of a thick slab of LaBi normal to the [111]-direction, finding three surface Dirac cones near three M s in the surface Brillouin zone (SBZ).

Our first-principles calculations are implemented in the VASP package with the generalized gradient approximation (GGA) and the projector augmented wave (PAW) method [26–28]. Lattice constants of rock salt lanthanum monopnictides are adopted from experimental values [29–33]. A Monkhorst-Pack k-mesh ($11 \times 11 \times 11$) is used to sample the Brillouin zone [34]. Fig.1(a) shows the BZ of the lanthanum monopnictides. To account for the electron-electron interaction, a mean field Hubbard correction term (U) is introduced into the frame of density functional theory[35] (DFT+U). The absence of f -electrons and the significant dispersion of $5d$ -states in all compounds suggest the itinerant nature of the conduction band. In accordance with this observations, it is found in our calculation that when $U < 0.5\text{eV}$, the lattice constants obtained are consistent with the experimental values. We hence choose $U = 0.25\text{eV}$ for all calculations performed in this work. We also note that there is no qualitative difference between the results for $U = 0$ and $U = 0.5\text{eV}$.

The band structure along high-symmetry lines for LaN in the absence of SOC is plotted in Fig.2(a). A band inversion at X is seen. The p_x states of N is about 45meV higher than the d_{yz} states of La. Due to the opposite parity of the two orbitals, the band inversion would have indicated a 3D TI if the direct gap were nonzero. However, there are two band crossing points near X: one along ΓX and the other along XW . A symmetry analysis shows that neither of them is a discrete crossing point in BZ, but each is an intersection of two nodal rings, protected by mirror symmetries. There are three mirror planes: M_{yz} that maps x to $-x$, M_{xz} that maps y to $-y$ and M_{xy} that maps z to $-z$. Let us focus on M_{xy} for now. In the BZ, bands on the plane defined by $k_z = 0$ can be labeled by the eigenvalues of M_{xy} , $m_{xy} = \pm 1$. A band with $m_{xy} = +1$ cannot anti-cross another band with $m_{xy} = -1$, because any hybridization would break mirror symmetry. This is exactly our case: p_x -orbital is invariant under m_{xy} thus having $m_{xy} = +1$, while d_{yz} -orbital has $m_{xy} = -1$. Hence, on the $k_z = 0$ -plane, the conduction band and valence band cross each other in

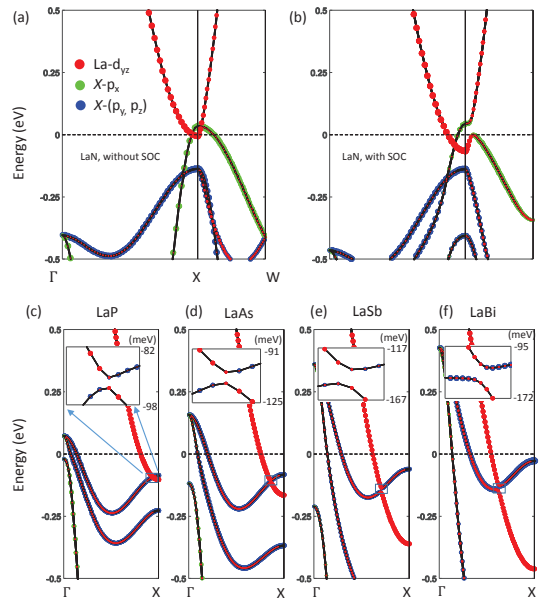


FIG. 2: Band structures of $\text{La}X$ with orbital analysis. (a,b)The band structure of LaN in the absence and the presence of SOC, respectively. (c-f) The band structures of LaP, LaAs, LaSb and LaBi along ΓX , respectively, in the presence of SOC, with insets showing details of the anti-crossing.

a nodal ring, passing through ξ_1 . Similar analysis proceeds for the M_{xz} mirror plane and we derive another nodal ring on the $k_y = 0$ -plane also passing through ξ_1 . Therefore, ξ_1 is the intersection of two nodal rings. We can similarly deduce that ξ_2 is also such an intersection of two nodal rings, protected by M_{xz} and M_{yz} respectively. From symmetry analysis, we have already deduced three nodal rings that are all centered at X and cross each other at $\xi_{1,2}$ and their symmetry equivalents, as shown in the schematic in Fig.1(b). An extensive DFT calculation away from high-symmetry lines confirms this prediction, and the calculated configurations of the nodal rings are found in Fig.1(c,d).

We substantiate the above analysis by deriving a minimal $k \cdot p$ -Hamiltonian around X -point. Without SOC, there are two bands at X -point, so the $k \cdot p$ is given by a two-by-two matrix as function of $\mathbf{q} \equiv \mathbf{k} - X$, which can be decomposed as the sum of the identity matrix and three Pauli matrices with \mathbf{q} dependent coefficients:

$$h(\mathbf{q}) = \sum_{\mu=0,x,y,z} d_{\mu}(\mathbf{q}) \sigma_{\mu}. \quad (1)$$

Since we are interested in the band crossing, the σ_0 -term, which represents an overall kinetic energy, can be neglected henceforth. The little group of X -point, formed by all symmetry operations that leave X -point invariant, gives symmetry constraints on the functional forms of $d_{i=x,y,z}(\mathbf{q})$. The little group is $D_{4h} \otimes \{I, T\}$, where $\{I, T\}$ is the group generated by time-reversal operation,

T . The generators of the little group include: fourfold rotation about x -axis C_{4x} , mirror plane M_{xy} , 3D inversion P and time-reversal T . The symmetry constraints hence take the form

$$\begin{aligned} C_{4x}h(q_x, q_y, q_z)C_{4x}^\dagger &= h(q_x, -q_z, q_y), \\ M_{xy}h(q_x, q_y, q_z)M_{xy}^\dagger &= h(q_x, q_y, -q_z), \\ Ph(\mathbf{q})P^\dagger &= h(-\mathbf{q}), \\ Th(\mathbf{q})T^\dagger &= h^*(-\mathbf{q}), \end{aligned} \quad (2)$$

where in the last equation we have used the fact that time-reversal is anti-unitary. If the basis vectors are chosen to be $|p_x\rangle$ for isospin up and $|d_{yz}\rangle$ for isospin down, the symmetry operations correspond to the following matrices: $C_{4x} = \sigma_z$, $M_{xy} = \sigma_z$, $P = -\sigma_z$ and $T = \sigma_0$. Substituting these into Eqs.(2), we obtain the following constraints for $d_i(\mathbf{q})$'s:

$$\begin{aligned} d_x &= 0, \\ d_y(\mathbf{q}) &= uq_x q_y q_z + O(q^5), \\ d_z(\mathbf{q}) &= m - uq_x^2 - v(q_y^2 + q_z^2) + O(q^4). \end{aligned} \quad (3)$$

The dispersion of Eq.(1) is $\sqrt{d_x^2 + d_y^2 + d_z^2}$, so the nodal points are determined by $d_x = d_y = d_z = 0$. The explicit forms of $d_i(\mathbf{q})$'s given in Eqs.(3) immediately yield three nodal rings: one circle given by $q_x = 0$, $q_y^2 + q_z^2 = m/v$, one ellipse given by $q_y = 0$, $uq_x^2 + vq_z^2 = m$ and another ellipse given by $q_z = 0$, $uq_x^2 + vq_y^2 = m$.

The linked nodal rings are, however, generically unstable against perturbative SOC, i.e., the conduction and the valence bands anti-cross, despite the unbroken mirror symmetry. This is because the above mentioned mirror symmetries, which only act in the spatial degrees of freedom, are no longer symmetries of the system, as the spatial degrees of freedom are now coupled to the spin degrees of freedom by SOC. A ‘real’ mirror symmetry acts simultaneously on the spatial and the spin spaces: M_{xy} , for example, not only sends z to $-z$, but also sends $s_{x,y}$ to $-s_{x,y}$, i.e., performs a π -rotation about y -axis in the spin space, because spin is a pseudo vector. With the additional spin-rotation, each band with mirror eigenvalue m_\pm in the non-SOC system becomes two degenerate bands with mirror eigenvalues $+im_\pm$ and $-im_\pm$ for the spin-up and spin-down sub-bands, respectively. Therefore, the band crossing between p_x band and d_{yz} band on $k_z = 0$ -plane is no longer protected by M_{xy} : the spin-up (spin-down) sub-band of p_x has the same eigenvalue of M_{xy} as the spin-down (spin-up) sub-band of d_{yz} and they will anti-cross. The nodal rings hence disappear generically. However, the crossing point ξ_1 along ΓX remains gapless for another symmetry reason. The high-symmetry line ΓX is a C_{4x} -invariant line, meaning that each band along this line can be labeled by its C_{4x} eigenvalue. With SOC, C_{4x} is composed of fourfold rotations in both the spatial and the spin spaces. According to this definition, the two sub-bands of the p_x band

have C_{4x} eigenvalues of $e^{\pm i\pi/4}$, and those of the d_{yz} band have eigenvalues of $-e^{\pm i\pi/4}$. Therefore, the two doublet bands can still cross each other as they have different C_4 -eigenvalues and the four-band crossing point, ξ_1 , as well as its time-reversal equivalent, are two 3D Dirac points. In Fig.2(b), it is confirmed in calculation that while the crossing at ξ_2 opens a gap, ξ_1 remains gapless.

The analysis can also be made explicit in the $k \cdot p$ -theory. $h(\mathbf{q})$ in Eq.(1) only involves the orbital degrees of freedom, and we need to find the terms coupling the orbital and the spin degrees of freedom, i.e., SOC terms, allowed by the little groups. As explained above, all point group operations (except for 3D inversion which does not act on spin) are now constituted of a spatial part and a spin rotation. One should also remember that time-reversal acts nontrivially in the spin space, sending $\{| \uparrow \rangle, | \downarrow \rangle\}$ to $\{| \downarrow \rangle, | -\uparrow \rangle\}$. If the basis vectors are chosen to be $\{|p_x, \uparrow\rangle, |p_x, \downarrow\rangle, |d_{yz}, \uparrow\rangle, |d_{yz}, \downarrow\rangle\}$, the little group generators take the form: $C_{4x} = \sigma_z \exp(-is_x\pi/4)$, $M_{xy} = -i\sigma_z s_z$, $P = \sigma_z$ and $T = K(is_y)$, where $s_{x,y,z}$ are Pauli matrices acting on the real spin, in contrast to $\sigma_{x,y,z}$ that act on the isospin. Under the symmetry constraints in Eqs.(2), we find the following SOC terms are allowed

$$H_{soc} = \lambda\sigma_x(q_y s_y - q_z s_z) + O(q^3). \quad (4)$$

With SOC terms added, the dispersion becomes

$$E = \sqrt{[m - uq_x^2 - v(q_y^2 + q_z^2)]^2 + \lambda^2(q_y^2 + q_z^2)}, \quad (5)$$

whose only band crossing points are given by $q_y = q_z = 0$ and $q_x^2 = m/u$.

Now we move down the pnictogen in the table of element, from N to P and further down to As, Sb and Bi. We notice that the lattice constant increases drastically from 5.3\AA to 6.03\AA in LaP, then gradually increases up to 6.58\AA in LaBi. This change modifies the bands near X -point significantly: it pushes the pnictogen p_x -band down in energy by a large amount, such that the valence band becomes the $p_{y,z}$ doublet (without SOC). Upon adding SOC, the $p_{y,z}$ -bands (now four bands including spin) split into a lower band of $J_z = \pm 1/2$, consisting of $|p_y + ip_z, \downarrow\rangle$ and $|p_y - ip_z, \uparrow\rangle$ state and a higher band of $J_z = \pm 3/2$ consisting of $|p_y + ip_z, \uparrow\rangle$ and $|p_y - ip_z, \downarrow\rangle$ state. As a combined result of lattice and SOC, we find that while the band inversion also happens at X -point between the La d -states and the pnictogen p -states, the band crossing along ΓX becomes an anti-crossing. See Fig.2(c-f). The gap at the anti-crossing point is as small as $\sim 3\text{meV}$ in LaP, increasing to 6meV , 20meV and 35meV in LaAs, LaSb and LaBi, respectively. The anti-crossing can again be understood in a symmetry analysis. Per the definition of above, the $J_z = \pm 3/2$ states have C_4 -eigenvalues of $-e^{\pm i\pi/4}$, same as those of the d_{yz} -states: C_4 -symmetry can no longer protect their crossing. Here we see that the change in the orbital nature of the valence band induces

a topological phase transition from a Dirac semimetal to a 3D TI.

An effective $k \cdot p$ theory can be established to confirm this result and be used to gain more information. If we the four basis vectors are $\{|p_y + ip_z, \rightarrow\rangle, |p_y - ip_z, \leftarrow\rangle, |d_{yz}, \rightarrow\rangle, |d_{yz}, \leftarrow\rangle\}$, where \rightarrow / \leftarrow means the spin is along positive/negative x -directions, the generators of the little group are represented by $C_{4x} = \exp(-i3\sigma_z s_x \pi/4)$, $M_{xy} = i\sigma_z s_z$, $P = -\sigma_z$ and $T = -K(i\sigma_0 s_y)$. The generic form (up to the first order of \mathbf{q}) of the $k \cdot p$ theory is

$$H(\mathbf{q}) = M\sigma_z + r_1 q_x \sigma_x s_x + r_2 \sigma_y (s_y q_y - s_z q_z). \quad (6)$$

The dispersion of this Hamiltonian is fully gapped, and since the parity of the occupied states at $\mathbf{q} = 0$ changes as M changes sign, we see that a band inversion at X changes the strong Z_2 index of the system according to the Fu-Kane formula[36]. The explicit form in Eq.(6) also enables us to calculate the change in the mirror Chern number[37, 38] when the band inversion happens, i.e., when M changes sign. There are three independent mirror planes to consider: M_{xy} , M_{yz} and M_{011} , where M_{011} is the plane rotated from M_{yz} by 45 degrees about x -axis. Note that although M_{xy} and M_{yz} are related by C_{4z} in the whole BZ, they are *not* related by any little group operation at X -point, and are hence independent operations. A straightforward calculation shows that the change in the three mirror Chern numbers, as m changes from positive to negative, are given by

$$\begin{aligned} \Delta C_{xy} &= \Delta C_{011} = 1, \\ \Delta C_{yz} &= \text{sign}(r_1 r_2). \end{aligned} \quad (7)$$

While $\text{La}X$ is predicted to be a 3D TI when $X = \text{P, As, Sb}$ and Bi , a single surface Dirac cone may only exist on certain surface terminations, due to the large hole pocket near Γ . To see this point, let us consider the (001)-surface. Since there are an odd number of surface Dirac cones, there must be one Dirac cone at \bar{M} or at $\bar{\Gamma}$ in the SBZ. At the same time, we notice that in the 3D BZ, the line projecting to \bar{M} passes two X -points, thus having two band inversions. Therefore a single Dirac cone cannot exist at \bar{M} . $\bar{\Gamma}$ -point in SBZ is the projection of the line ΓX in BZ, having only one band inversion, but in Fig.2(c-f), we see that along this line the indirect gap is closed, i.e., collapsing the bands to one point results in a continuous spectrum. Therefore the single Dirac cone is buried inside the bulk projection continuum and hence cannot be observed.

So far we have argued that no single Dirac cone appears on the (001)-surface. The topological surface state can, however, be observed on the (111)-surface. The four time-reversal invariant momenta are $\bar{\Gamma}$ and three \bar{M} 's, and either there is one Dirac cone at $\bar{\Gamma}$ or there are three Dirac cones at three \bar{M} 's. In Fig.1(a), we notice the following projections from lines in BZ to points in SBZ:

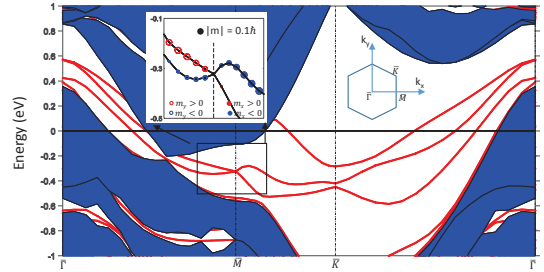


FIG. 3: The band structure on the (111)-surface of a 20-layer slab of LaBi. The inset shows the spin texture near \bar{M} .

$\Gamma L_4 \rightarrow \bar{\Gamma}$ and $X_i L_i \rightarrow \bar{M}_i$. The band inversion happens at all X , so according to the projection, we expect three Dirac cones at three \bar{M} 's. The prediction is supported by calculation on a 20-layer LaBi slab normal to the [111]-direction. In Fig.3, we see a spin-split Dirac cone at \bar{M} . Due to the spin-orbital coupling, the spin degrees of freedom are entangled with orbital degrees of freedom, and therefore while the surface bands are spin-split, the physical spins are not fully polarized.

To conclude, we theoretically predict topological semimetals as well as topological insulators in lanthanum monopnictides with rock salt structure, $\text{La}X$ ($X = \text{N, P, As, Sb}$ and Bi). We identify LaN as a nodal ring semimetal when spin-orbital coupling is neglected; and starting from this phase, we use analysis and numerics to show that it becomes a 3D Dirac point when perturbative spin-orbital coupling is taken into account. Moving down in the pnictogen column, we find LaP , LaAs , LaSb and LaBi to be 3D topological insulators. Our calculation shows that the topological transition from Dirac semimetal to topological insulator is induced by the change in the orbital character of the valence band caused by an increase in the lattice constant. We further argue that the topological surface states of these 3D topological insulators cannot be observed on the certain surfaces such as (001)-surface but may be observed on the (111)-surface. We calculate the surface states in a LaBi (111)-slab as demonstration.

The work at National University of Singapore is supported by the National Research Foundation, Prime Minister's Office, Singapore under its NRF fellowship (NRF Award No. NRF-NRFF2013-03). The work at Massachusetts Institute of Technology is supported by the Science and Technology Center for Integrated Quantum Materials, NSF Grant No. DMR-1231319 (CF), and the DOE Office of Basic Energy Sciences, Division of Materials Sciences and Engineering under Award No. de-sc0010526 (LF).

[†]These two authors contribute equally to this work.

*nilnish@gmail.com

**liangfu@mit.edu

-
- [1] S. M. Young, S. Zaheer, J. C. Y. Teo, C. L. Kane, E. J. Mele, and A. M. Rappe, Phys. Rev. Lett. **108**, 140405 (2012).
- [2] Z. Wang, Y. Sun, X.-Q. Chen, C. Franchini, G. Xu, H. Weng, X. Dai, and Z. Fang, Phys. Rev. B **85**, 195320 (2012).
- [3] Z. Wang, H. Weng, Q. Wu, X. Dai, and Z. Fang, Phys. Rev. B **88**, 125427 (2013).
- [4] X. Wan, A. M. Turner, A. Vishwanath, and S. Y. Savrasov, Phys. Rev. B **83**, 205101 (2011).
- [5] A. A. Burkov and L. Balents, Phys. Rev. Lett. **107**, 127205 (2011).
- [6] A. Go, W. Witczak-Krempa, G. S. Jeon, K. Park, and Y. B. Kim, Phys. Rev. Lett. **109**, 066401 (2012).
- [7] L. Lu, L. Fu, J. D. Joannopoulos, and M. Soljacic, Nature Photonics (2013).
- [8] H. Weng, C. Fang, Z. Fang, B. A. Bernevig, and X. Dai, Phys. Rev. X **5**, 011029 (2015).
- [9] S.-M. Huang, S.-Y. Xu, I. Belopolski, C.-C. Lee, G. Chang, B. Wang, N. Alidoust, G. Bian, M. Neupane, A. Bansil, et al., arXiv preprint arXiv:1501.00755 (2015).
- [10] Z. K. Liu, J. Jiang, B. Zhou, Z. J. Wang, Y. Zhang, H. M. Weng, D. Prabhakaran, S.-K. Mo, H. Peng, P. Dudin, et al., Nat. Mater **13**, 677 (2014).
- [11] Z. K. Liu, B. Zhou, Y. Zhang, Z. J. Wang, H. M. Weng, D. Prabhakaran, S.-K. Mo, Z. X. Shen, Z. Fang, X. Dai, et al., Science (2014).
- [12] M. Neupane, S.-Y. Xu, R. Sankar, N. Alidoust, G. Bian, C. Liu, I. Belopolski, T.-R. Chang, H.-T. Jeng, H. Lin, et al., Nat. Comm. **5** (2014).
- [13] S.-Y. Xu, C. Liu, S. K. Kushwaha, R. Sankar, J. W. Krizan, I. Belopolski, M. Neupane, G. Bian, N. Alidoust, T.-R. Chang, et al., Science **347**, 294 (2015).
- [14] S.-Y. Xu, C. Liu, S. Kushwaha, T.-R. Chang, J. Krizan, R. Sankar, C. Polley, J. Adell, T. Balasubramanian, K. Miyamoto, et al., arXiv:1312.7624 (2013).
- [15] L. Lu, Z. Wang, D. Ye, L. Ran, L. Fu, J. D. Joannopoulos, and M. Soljacic, arXiv:1502.03438 (2015).
- [16] S.-Y. Xu, I. Belopolski, N. Alidoust, M. Neupane, C. Zhang, R. Sankar, S.-M. Huang, C.-C. Lee, G. Chang, B. Wang, et al., arXiv:1502.03807 (2015).
- [17] B. Lv, H. Weng, B. Fu, X. Wang, H. Miao, J. Ma, P. Richard, X. Huang, L. Zhao, G. Chen, et al., arXiv preprint arXiv:1502.04684 (2015).
- [18] B.-J. Yang, M. S. Bahramy, R. Arita, H. Isobe, E.-G. Moon, and N. Nagaosa, Phys. Rev. Lett. **110**, 086402 (2013).
- [19] S. Murakami, New Journal of Physics **9**, 356 (2007).
- [20] G. Y. Cho, arXiv preprint arXiv:1110.1939 (2011).
- [21] T. Das, Phys. Rev. B **88**, 035444 (2013).
- [22] B. Dora, I. F. Herbut, and R. Moessner, Phys. Rev. B **88**, 075126 (2013).
- [23] G. B. Halasz and L. Balents, Phys. Rev. B **85**, 035103 (2012).
- [24] J.-M. Hou, Phys. Rev. Lett. **111**, 130403 (2013).
- [25] H. Weng, Y. Liang, Q. Xu, Y. Rui, Z. Fang, X. Dai, and Y. Kawazoe, arXiv:1411.2175 (2014).
- [26] M. Payne, M. Teter, D. Allan, T. Arias, and J. Joannopoulos, Rev. Mod. Phys. **64**, 1045 (1992).
- [27] I. Robertson, M. Payne, and V. Heine, J. Phys.-Condes. Matter **3**, 8351 (1991).
- [28] J. Perdew and Y. Wang, Phys. Rev. B **45**, 13244 (1992).
- [29] G. L. Olcese, J. Phys. F **9**, 569 (1979).
- [30] S. Ono, K. Nomura, and H. Hayakawa, J. Less-Common MET. **38**, 119 (1972).
- [31] K. Yoshihara, J. Taylor, L. Calvert, and J. Despault, J. Less-Common MET. **41**, 329 (1975).
- [32] T. Palewski, J. Warchulska, and L. Pawlak, Phys. Status Solidi A-Appl. Res. **137**, 45 (1993).
- [33] J. Leger, D. Ravot, and J. Rossatmignod, J. Phys. C **17**, 4935 (1984).
- [34] H. Monkhorst and J. Pack, Phys. Rev. B **13**, 5188 (1976).
- [35] S. L. Dudarev, G. A. Botton, S. Y. Savrasov, C. J. Humphreys, and A. P. Sutton, Phys. Rev. B **57**, 1505 (1998).
- [36] L. Fu and C. L. Kane, Phys. Rev. B **76**, 045302 (2007).
- [37] J. C. Y. Teo, L. Fu, and C. L. Kane, Phys. Rev. B **78**, 045426 (2008).
- [38] T. H. Hsieh, H. Lin, J. Liu, W. Duan, A. Bansil, and L. Fu, Nature Communications **3**, 982 (2012).